On the formation of U-Al alloys in the molten LiCl-KCl eutectic

L. Cassayre[a], C. Caravaca[b], R. Jardin[c], R. Malmbeck[c*], P. Masset[c], E. Mendes[c], J. Serp[c***], P. Soucek[c], J.-P. Glatz[c]**

a) Laboratoire de Génie Chimique (LGC), Université Paul Sabatier, UMR CNRS 5503, 31062 Toulouse Cedex 9, France
b) CIEMAT, DE/DFN/URAA, Avda. Complutense, 22. Madrid 28040, Spain
c) European Commission, JRC, Institute for Transuranium Elements, P.O. Box 2340, 76125 Karlsruhe, Germany

Abstract

U-Al alloy formation has been studied in the temperature range of 400 – 550 °C by electrochemical techniques in the molten LiCl-KCl eutectic. Cyclic voltammetry showed that underpotential reduction of U(III) onto solid Al occurs at a potential about 0.35 V more anodic than pure U deposition. Open circuit potential measurements, recorded after small depositions of U metal onto the Al electrode, did not allow the distinction between potentials associated with UAl_x alloys and the Al rest potential, as they were found to be practically identical. As a consequence, a spontaneous chemical reaction between dissolved UCl_3 and Al is thermodynamically possible and was experimentally observed. Galvanostatic electrolyses were carried out both on Al rods and Al plates. Stable and dense U-Al deposits were obtained with high faradic yields, and the possibility to load the whole bulk of a thin Al plate was demonstrated. The analyses (by SEM-EDX and XRD) of the deposits indicated the formation of different intermetallic phases (UAl_2, UAl_3 and UAl_4) depending on the experimental conditions.

1

*Corresponding author. Tel +49 7247 951 376; Fax +49 7247 951 99611.

E-mail address: rikard.malmbeck@ec.europa.eu

** present address: Karl-Winnacker-Institut der Dechema e.V., Theodor-Heuss-Allee 25, 60486 Frankfurt am Main, Germany.

*** present address: CEA / Centre de Valduc, DAM/DTMN/SRPu, 21120 Is sur Tille, France

1. Introduction

The reprocessing of nuclear fuels today aims primarily to recycle the major actinides (An: U, Pu). Main objectives for future reactor systems are an effective fuel utilization and waste minimization through recycling of all actinides. This is why reprocessing systems that include also the recovery of heavier actinides, the so-called minor actinides (MA: Np, Am, Cm) are being developed. At present, pyrochemical techniques are investigated world-wide in molten chlorides and fluorides salts for the grouped separation of actinides from the fission products. Especially an effective separation of the An from lanthanides (Ln) is important, mainly because of their neutron poisoning properties and from the material burden. In spent nuclear fuels, the Ln content might be up to 50 times that of Am/Cm.

Electrorefining is the most developed pyrochemical separation process which is used in the USA for sodium-cooled fast breeder reactor metallic fuels in the IFR (Integral Fast Reactor) concept [1]. In this process, uranium is separated from the bulk of fission products by electrolysis in a molten salt electrolyte onto a solid inert cathode. Further developments aim to simultaneously recover U, Pu and the MA by electrorefining onto a liquid Cd cathode [2, 3], leaving fission products in the salt phase. The main advantage

using Cd is the stabilisation of the reactive actinide metals as An-MA-Cd alloy and that a recovery of actinides in the metallic state for fuel fabrication is possible after a Cd distillation step [4]. However, from a thermodynamical point of view, Cd is not the optimal metallic solvent to accomplish a good decontamination from Ln. To obtain as high separation factors as possible, the best solvent is the one in which the ratio of the activity coefficients is as low as possible. Among the metals in which activity coefficients of Pu, U and Ce are known [5, 6], liquid as well as solid aluminium proves to be the most promising solvent for the separation of An from Ln [7]. This is the reason why additional separation systems are now being developed such as reductive extraction of An into a molten Al solvent in fluoride media [8] and electrodeposition or co-deposition of An onto solid Al cathodes in a molten chloride salt [9]. In these processes An are recovered as stable An-Al alloys.

Some aspects of the electrolytic process in chloride media, developed in ITU, have already been presented in previous articles [9, 10]. This paper is focused on the extraction of dissolved U^{3+} from molten LiCl-KCl by alloying uranium onto aluminium by electrodeposition at potentials more positive than the pure uranium deposition potential. The U-Al alloy formation has been studied by electrochemical techniques in the LiCl-KCl eutectic, in the 400-550°C temperature range, and the thermochemical properties of the system are discussed. In addition, gram-scale galvanostatic electrolyses have been performed onto Al rod and plate electrodes. Characterisations of the cross-section of the deposits were carried out using scanning electron microscopy with energy dispersive X-ray (SEM-EDX) and X-ray diffraction (XRD) in order to investigate the thickness and composition of the alloy formed.
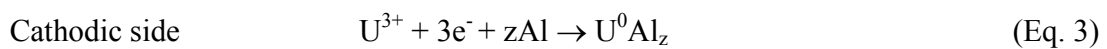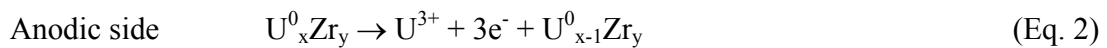
2. Experimental

The experimental set-up for the electrochemical measurements has been described in a previous paper [11]. Several electrolytic baths consisting of a mixture of 30 to 40 g of anhydrous LiCl-KCl eutectic (Aldrich 99.99 %) containing U^{3+} (1.00-1.60 mass.%) were prepared by oxidising uranium metal. The metal was introduced in a molten Bi phase in the bottom of the crucible and oxidised by adding $BiCl_3$ to the salt phase at a temperature of 450 °C. Stirring of the salt phase by Ar gas bubbling and a temperature increase to 550 °C were used to complete the reaction. The redox reaction for uranium is given by:

$$U^0_{Bi-phase} + Bi^{3+}_{salt-phase} \Leftrightarrow U^{3+}_{salt-phase} + Bi^0_{Bi-phase} \qquad \text{(Eq. 1)}$$
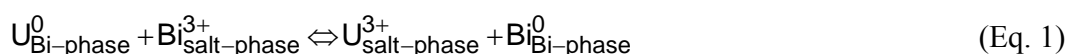
Electrochemical measurements were carried out in a cell equipped with a three-electrode set-up and a PAR 273 potentiostat with EG&G M270 electrochemical software. Working electrodes made of tungsten or aluminium wires (1 mm diameter) were dipped approximately 5 mm into the bath. The reference electrode used was a LiCl-KCl-AgCl (1 mass.%)/Ag prepared in a PYREX glass tube (written as AgCl/Ag in the rest of the text) and the auxiliary electrode was a Mo wire (1 mm diameter) bent into the shape of a spiral.

Uranium electrodepositions were carried out in LiCl-KCl-UCl_3 melts by applying a constant current between pieces of U-Zr alloy (80/20 mass.%) placed in an inert Ta anode basket, and aluminium cathodes (either plates or rods), as illustrated in Figure 1.

The amount of U-Zr loaded into the anode basket (typically 2-3 g) was always in excess compared to the amount of U dissolved by anodic oxidation, in order to prevent Zr oxidation (U is selectively dissolved since it is less noble than Zr [12]). The expected electrochemical reactions in the case of U electrodeposition are the following:

Anodic side $\qquad U^0_x Zr_y \rightarrow U^{3+} + 3e^- + U^0_{x-1} Zr_y$ (Eq. 2)

Cathodic side $\qquad U^{3+} + 3e^- + zAl \rightarrow U^0 Al_z$ (Eq. 3)

During electrodeposition, cathodic, anodic and cell potentials were monitored and samples (about 100 mg) were taken from the salt phase before and after each electrolysis. Salt samples were dissolved in 1 M nitric acid and the concentration of U^{3+} was determined both by ICP-MS analysis and by the non-destructive XRF method [13]. After each electrolysis, the Al electrode was removed from the bath and allowed to stay at elevated temperature above the salt melt, 12 hours or more, in order to let adhered salt drip off. After cooling, the remaining adhered salt was removed by repeated washing in an ultra-sonic bath, using a water-ethanol mixture (10/90 vol %). The electrodes were then cut, embedded in resin and surface polished for further surface analysis of the cross-sections by SEM coupled with EDX measurements.

In one case, the deposit was scratched from the electrode, ground and embedded in an epoxy resin. Precise X-ray powder diffraction analysis was performed on a Siemens D8 advanced diffractometer (Bragg-Bentano configuration) equipped with a Ge(111) incident beam monochromator and a VANTEC position sensitive detector, covering 6° in 2θ. For the structure refinement and the quantitative phase analysis by the Rietveld

method, the XRD patterns were typically collected in the 2θ range of 10-110° (step size

of 0.0085°), with an exposure time of 5 s per step. Samples were rotated during the data

collection in order to improve the sample statistic and reduce the effects of possible

preferred orientation. The fitting and refinement were performed using the Fullprof

program.

3. Results and discussion

3.1 Electrochemical study

Figure 2 shows two voltammograms recorded in a UCl_3-containing LiCl-KCl salt on

tungsten and aluminium working electrodes.

On the tungsten electrode, U^{3+} ions are reduced to U metal in one step involving the

transfer of three electrons [14, 15]. At 460°C, this reduction peak (Ep_{Ic}) is observed at a

potential of −1.52 V vs. AgCl/Ag, and associated with a sharp reoxidation peak (Ep_{Ia}) at -

1.20 V vs. AgCl/Ag, corresponding to the dissolution of the deposited U metal during the

cathodic sweep. At potentials more positive than the U^{3+}/U^0 redox couple, a wave with a

shape characteristic of a soluble-soluble transition is observed; it corresponds to the

U^{4+}/U^{3+} redox couple [14, 15].

Using an Al working electrode (Figure 2, bold curve), two redox systems were observed.

The first cathodic peak at Ep_{IIc} = -1.11 V vs. AgCl/Ag is attributed to the formation of a

U-Al alloy. Due to the alloy formation, the electrodeposition of U^{3+} on Al occurs at a

more anodic potential compared to the inert W cathode. A similar behaviour has been reported on Al electrodes for other actinides (Am and Pu [9]) and for several lanthanides [16-18].

The second peak, Ep_{Ic}, corresponds to the reduction of U^{3+} to pure U metal; it commences at the same potential as on the inert W electrode.

On the anodic side, the electrochemical window is limited by the oxidation of Al occurring at a potential of about -1.00 to -0.90 V vs. AgCl/Ag and thereby hiding the reoxidation peak of the U-Al alloy.

Cyclic voltammograms were recorded on solid Al at different scan rates (Figure 3). The value of the potential Ep_{IIc} is shifted towards negative values when the scan rate is increased up to the polarization rate of 100 mV.s^{-1} (for each temperature studied). According to the literature [19], it indicates that the system shows irreversibility.

Temperature dependence

Figure 4 shows forward sweeps recorded on an Al electrode at four temperatures between 400°C and 550°C at a low scan rate (10 mV.s^{-1}). The alloying rate is strongly temperature dependent, since the current density of the reaction increases with temperature. The reason is likely to be the faster interdiffusion of U and Al atoms at higher temperature, leading to a greater current for the formation of the alloy. The rest potential as well as the reduction peak (Ep_{IIc}) are slightly shifted towards more positive potentials when the temperature is increased, which is partly due to a shift of the AgCl/Ag reference electrode according to the Nernst equation.

Open-circuit potential (OCP) curves

Open circuit chonopotentiometry technique was used in an attempt to identify the U-Al

intermetallic compounds formed in LiCl-KCl and to determine their standard Gibbs

energy of formation, as described for instance in [20, 21]. After a short polarization, at a

potential corresponding to the electrodeposition of U metal, the open circuit potential was

recorded vs. time (Figure 5) for T=450°C. Similar curves were obtained for all

temperatures tested, in the range 450-550°C.

The E-t curves show a first potential plateau at ~ -1.33 V vs. AgCl/Ag, which

corresponds to the U(III)/U equilibrium potential:

$$UCl_{3(dissolved)} + 3e^- = U_{(s)} + 3\ Cl^- \hspace{3cm} \text{(Eq. 4)}$$
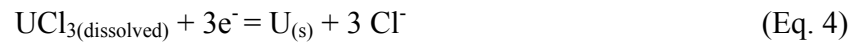
The OCP curves obtained with the same experimental method on other systems (e.g.

Lanthanides-Al in LiCl-KCl [20]) usually show a succession of plateaus corresponding to

the equilibrium between different intermetallic compounds, but it was not the case for the

U-Al system. The second plateau at ~ -1.00 V vs. AgCl/Ag can indeed not be resolved

from the rest potential of the Al electrode in this melt.

It was assumed that the second plateau corresponds to an equilibrium between Al and the

UAl_n alloy, with n equal to 2, 3 or 4 since the U-Al system exhibits three intermetallic

compounds [22], and that the Al and the U-Al alloy equilibrium potentials are practically

the same. The corresponding half cell reaction is:

$$UCl_{3(dissolved)} + 3e^- + n\ Al_{(s)} = UAl_{n(s)} + 3\ Cl^- \hspace{2cm} \text{(Eq. 5)}$$
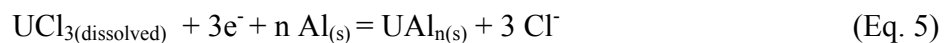
The standard Gibbs energy of formation of UAl_n was then derived from the potential difference ΔE_{UAln} between the plateaus related to the equilibrium U(III)/U and U(III)/UAl_n+Al. It corresponds to the reaction:

$$U_{(s)} + n\ Al_{(s)} = UAl_{n(s)} \qquad\qquad (Eq.\ 6)$$

since (Eq. 6) = (Eq. 5) – (Eq. 4).

The standard free energy of formation of UAl_n was then calculated using the expression:

$$\Delta G_f^\circ\ (UAl_n) = -3\ F\ \Delta E_{UAln} \qquad\qquad (Eq.\ 7)$$

Data obtained in the 400-550°C temperature range are given in Table 1.

The standard Gibbs energy values are compared in Table 1 to tabulated data compiled by Kassner [22] and mostly derived from emf measurements by Chiotti on solid Al [23] and Lebedev above the melting point of Al [24] in the LiCl-KCl eutectic melt. Given the uncertainties in the measurements of ΔE_{UAln} and the small difference of Gibbs energy of formation between UAl_4 and UAl_3 (around 1 kJ.mol^{-1}), it can only be concluded from our OCP measurements that UAl_4 and/or UAl_3 is formed at the Al electrode.

With optimised conditions of deposition (i.e. duration, potential and temperature) before recording the relaxation, the OCP technique usually allows observing a plateau for each intermetallic compound of the binary system. Thus a plateau related to the presence of UAl_2 should be observed, but it was not the case with our experimental condition, maybe because the amount of deposited U was too small, or because the rate of deposition was too slow.

3.2 Spontaneous reaction

Both the shape of the cyclic voltammogram and the OCP measurements indicate that the U-Al alloy formation occurs at a potential very close to the $AlCl_3/Al$ equilibrium potential; a spontaneous redox reaction between UCl_3 and Al could therefore occur when solid Al is placed in contact with a molten salt containing dissolved UCl_3.

This was investigated by immersing an Al plate during 72 hours into 40 g of a LiCl-KCl-UCl_3 mixture containing 1.53 mass.% of U(III). After removal of the electrode from the melt and cleaning in an ethanol-water mixture, a metallic deposit was observed on the plate, as illustrated in Figure 6. The mass balance (i.e. the mass difference between the initial Al plate and the plate after immersion and cleaning) indicated a mass increase of 117 mg.

The deposit was brittle; it was scratched from the Al plate and weighted. The recovered mass was about 141 mg. The X-ray powder diffraction analysis of the deposit (Figure 7) was successfully indexed on the basis of two unit cells: one cubic (a = 4.2652 Å) and one orthorhombic (a = 4.3983 Å, b = 6.2489 Å, c = 13.729 Å) corresponding to UAl_3 and UAl_4, respectively [22]. Taking into account the number of formula units per cell and the molecular weight of each of the two phases, a weight ratio 68.7 % of UAl_3 and 31.4 % UAl_4 was determined. This clearly confirms the occurrence of a spontaneous chemical reaction leading to the formation of U-Al alloys.

Thermochemical considerations allow a better understanding of the system. In a first step, an evaluation of the spontaneous reaction was performed assuming the formation of 100% of pure UAl_3 by the reaction of solid Al in equilibrium with LiCl-KCl eutectic containing a given amount of UCl_3. The following reaction is considered:

$$UCl_{3(dissolved)} + 4\ Al_{(solid)} = UAl_{3(solid)} + AlCl_{3(dissolved)} \qquad [K_1] \qquad (Eq.\ 8)$$

Since Al and UAl_3 are pure and solid phases, the equilibrium constant K_1 associated with (Eq. 8) is equal to:

$$K_1 = \frac{a(AlCl_3)}{a(UCl_3)} = \exp\left(-\frac{\Delta_r G_1^{\circ}(T)}{RT}\right) \qquad (Eq.\ 9)$$

where R ($J.K^{-1}.mol^{-1}$) is the gas constant, T (K) the absolute temperature and $\Delta_r G^{\circ}_1$ ($J.mol^{-1}$) the standard Gibbs energy of the reaction associated with K_1.

The activities of UCl_3 and $AlCl_3$ are linked to their molar fraction X according to $a(UCl_3)=\gamma(UCl_3)\cdot X(UCl_3)$ and $a(AlCl_3)=\gamma(AlCl_3)\cdot X(AlCl_3)$, where γ is the activity coefficient in the LiCl-KCl eutectic. The relation between X_{AlCl3} and X_{UCl3} at equilibrium is then:

$$X(AlCl_3) = X(UCl_3) \cdot \frac{\gamma(UCl_3)}{\gamma(AlCl_3)} \cdot \exp\left(-\frac{\Delta_r G_1^{\circ}(T)}{RT}\right) \qquad (Eq.\ 10)$$

Considering that the concentrations of UCl_3 and $AlCl_3$ are low in the melt, the molar fraction of $AlCl_3$ at equilibrium is roughly equal to:

$$X(AlCl_3) \approx \frac{n(AlCl_3)}{n(LiCl) + n(KCl)} = \frac{n(AlCl_3) \cdot M_{salt}}{m_{salt}} \qquad (Eq.\ 11)$$

11

where $n(AlCl_3)$ is the amount of $AlCl_3$ in the salt (mol), M_{salt} the molar mass of the LiCl-KCl eutectic (55.58 g.mol^{-1}) and m_{salt} the total mass of salt (40 g).

Given that there was neither $AlCl_3$ nor UAl_3 in the system prior the immersion of the Al plate and according to the stoichiometry of (Eq. 8), the number of moles of UAl_3 produced is equal to the number of $AlCl_3$ moles:

$$n(UAl_3)=n(AlCl_3) \qquad \text{(Eq. 12)}$$

Combination of (Eq. 10), (Eq. 11) and (Eq. 12) finally leads to:

$$m(UAl_3) = m_{salt} \cdot \frac{M_{UAl3}}{M_{salt}} \cdot X(UCl_3) \cdot \frac{\gamma(UCl_3)}{\gamma(AlCl_3)} \cdot \exp\left(-\frac{\Delta_r G_1^{\circ}(T)}{RT}\right) \qquad \text{(Eq. 13)}$$

where M_{UAl3} is the molar mass of UAl_3 (319 g.mol^{-1}).

Since the formation of UAl_4 was also evidenced by XRD characterizations, the same relation was established considering the formation of UAl_4 instead of UAl_3 according to the following relation:

$$UCl_{3(dissolved)} + 5\ Al_{(solid)} = UAl_{4(solid)} + AlCl_{3(dissolved)} \qquad [K_2] \quad \text{(Eq. 14)}$$
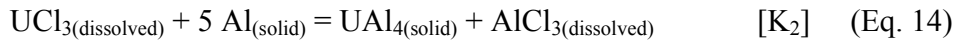
It leads to the expression of the amount of UAl_4:

$$m(UAl_4) = m_{salt} \cdot \frac{M_{UAl4}}{M_{salt}} \cdot X(UCl_3) \cdot \frac{\gamma(UCl_3)}{\gamma(AlCl_3)} \cdot \exp\left(-\frac{\Delta_r G_2^{\circ}(T)}{RT}\right) \qquad \text{(Eq. 15)}$$

where M_{UAl4} is the molar mass of UAl_4 (346 g.mol^{-1}) and $\Delta_r G^{\circ}_2$ (J.mol^{-1}) the standard Gibbs energy of reaction associated with K_2.

Calculations of the standard Gibbs energy $\Delta_r G°_1$ and $\Delta_r G°_2$ were performed at 450°C taking as reference state: Al(s), AlCl$_3$(liq), UCl$_3$(sc,liq), UAl$_3$(s) and UAl$_4$(s). The thermochemical data related to these compounds ($\Delta G_f°$ and activity coefficients in LiCl-KCl eutectic) are presented in Table 1 and Table 2.

The $\Delta_r G°$ values related to Eq. 8 and Eq. 14, reported in Table 3, are very close (difference of less than 2 kJ.mol^{-1}). This explains why both UAl$_3$ and UAl$_4$ are formed during the spontaneous reaction in our experimental conditions.

The masses of UAl$_4$ or UAl$_3$ at equilibrium were then evaluated according to Eq. 13 and Eq. 15. As detailed in Table 3, if pure UAl$_3$ is produced, the mass should be around 20 mg, while, in the case of UAl$_4$, a mass of 26 mg is expected. These calculations underestimate our experimental results by a factor of approximatively 7, since a mass increase of the Al plate of 117 mg was observed, corresponding to a mass of U-Al alloy between 157 mg (pure UAl$_3$) and 170 mg (pure UAl$_4$). This discrepancy might be caused by inaccurate values of the activity coefficients of UCl$_3$ or AlCl$_3$ used in the calculations. The overall calculation is nevertheless predicting the amount of U-Al with the right order of magnitude.

The spontaneous reductive extraction of U(III) onto solid Al is the major reaction occurring in the LiCl-KCl eutectic, and it is favored by the low activity of dissolved AlCl$_3$. The mass of U(III) extracted from the melt corresponds roughly to 20% of the initial amount of dissolved U, since a mass increase of the Al plate of 117 mg was

measured and the initial concentration of U(III) was 1.53 mass.% in 40 g of salt (i.e. 612 mg).

This spontaneous reaction has been mentioned earlier by Chiotti [23], who consequently used a low concentration of UCl_3 (1.3 mass.%) for the purpose of emf measurements in cells of the type $U_{(s)}$/KCl-LiCl-UCl_3/U-Al. Furthermore, it has been shown that the reaction is enhanced at higher temperatures (750-950°C), above the melting point of Al, in other chloride melts (NaCl-KCl for instance [28]), as well as in LiF-CaF_2 fluoride mixtures where U (as well as Pu and the MA) is fully extracted in a liquid Al phase at 830°C [7, 29].

3.3 Galvanostatic electrolysis

Galvanostatic electrolyses were carried out on Al rods and on Al plates (3 cm² < S < 5 cm²) in order to characterize the U-Al alloy formed by electrodeposition of U(III). As detailed in the experimental part, the anodic reaction consisted in the selective dissolution of U from a metallic U-Zr alloy.

A typical evolution of cathodic and anodic potentials during the electrolysis is shown in Figure 8. At the beginning, the current was gradually increased and adjusted until a stable cathodic potential was reached (~ -1.10 V vs. AgCl/Ag). This potential corresponds to the formation of a U-Al alloy as evidenced in section 3.1. During the course of the electrolysis, the cathodic potential decreased gradually (about 10 mV in total), probably because of the growth of the UAl_x layer which hindered the U-Al interdiffusion. After about 580 C passed, the cathodic potential sharply dropped and reached –1.40 V vs.

14

AgCl/Ag. At this point the cathode surface was saturated and could no longer alloy U at a rate of 40 mA. As a consequence, pure U started to be deposited onto the U-Al alloy surface. The electrolysis was then stopped.

Several electrolyses were carried out between 460°C and 550°C. The experimental conditions and the mass balances of the main electrolyses are summarized in Table 4.

The increase of mass of the Al cathode after the experiment (Δm) was compared to the expected mass (m_{th}). m_{th} was calculated from the imposed charge, assuming a 100% faradic yield, in order to estimate the reaction efficiency (R) according to:

$$R = \frac{\Delta m}{m_{th}}.100 \qquad\qquad\qquad \text{(Eq. 16)}$$

R is about 100% in the case of the Al plates, and even higher (~120%) with the Al rods. It shows that the reduction of U^{3+} ions onto solid Al is a faradic process. The reductive extraction of UCl_3 as well as the presence of salt inclusions in the alloy layer are likely to be the reasons why the increase of mass is greater than the theoretical value calculated by the Faraday's law.

3.4 Alloy characterization

Rods

Figure 9 shows the Al cathodes after the adhered salt was removed by ultra sonic bath washing in a water-ethanol mixture. In all runs, compact, metallic shiny and adherent U-Al surface deposits were formed.

Figure 10 shows a SEM micrograph of the cross-section of the Al rod from run 3. The deposit formed is a layer of about 500 μm thickness, having a very dense structure in the 50-100 μm layer close to the Al phase. Close to the surface, the U-Al alloy is in the form of large dendrites with salt inclusions between them. EDX mapping (Figure 10) confirmed the presence of a U-Al alloy phase, as well as salt inclusions by the presence of Cl.

EDX analysis also indicated that close to the pure Al phase the Al/U molar ratio is about 4 which indicates the formation of UAl_4 alloy. Further out a higher U content was found (Al/U close to 2.5), which may correspond to a mixture of UAl_3 and UAl_2 intermetallic compounds.

Zirconium was neither found in the deposit nor in the salt phase analysis during and after each electro-deposition test. It confirms that selective dissolution of U from U-Zr alloy at the anode had occurred.

Plates

The Al plates were characterized by SEM-EDX after electrolysis. In the case of runs U2 and U5 (Figure 11), a thick layer of alloy was evidenced on both sides of the plates, and the observations corresponding to the run U2 shows that almost all the Al electrode has reacted. The dense aspect of the U-Al deposits is very different from the highly dendritic morphology of pure U deposits obtained by electrodeposition of U(III) on various substrates in chloride melts [30].

The evaluated results from EDX measurements are summarized in Figure 12. EDX analysis confirmed the presence of an alloy layer consisting of U and Al in the molar ratio Al/U=2.5, which indicates a mixture of UAl_3 and UAl_2 alloys.

The Al/U molar ratio was found to be quite the same for each of the four electrodes analyzed and also independent of the distance from the electrode surface. This homogeneity might be the result of the experimental procedure: after each run, the electrodes were left above the melt for about 12 hours in order to let the adhered salt slip down. During this time, interdiffusion of Al and U atoms most probably occurred, leading to a homogenization of the alloy composition.

4. Conclusions

The U-Al alloy formation has been studied in the temperature range of $400 - 550 \, °C$ by electrochemical techniques. Cyclic voltammetry showed that underpotential reduction of U onto Al occurs, at a rate strongly dependent on temperature. Open circuit potential measurements, after small depositions of U metal onto the Al electrode, did not exhibit a

17

succession of plateau as usually observed during the relaxation of electrodeposited intermetallic compounds. This was attributed to the fact that the equilibrium potential of UAl_3 and UAl_4 with the melt was almost identical to the Al electrode rest potential. As a consequence a spontaneous chemical reaction between dissolved UCl_3 and Al is thermodynamically possible and this reaction was observed experimentally. Galvanostatic electrolyses were carried out both on solid Al rods and plates. Stable and dense U-Al deposits were obtained with a high current efficiency, and the possibility of loading the whole bulk of thin Al plates (0.5 mm in thickness) up to an average Al/U molar ratio of 2.5 was demonstrated. The quantitative analysis (by SEM-EDX and XRD) of the deposits indicated the presence of UAl_2, UAl_3 and UAl_4 depending on the experimental conditions.

References

[1]   H.F. McFarlane and M.J. Lineberry, Prog. Nucl. Energ., 31, 1/2 (1997) 155-173.

[2]   M. Iizuka, K. Uozumi, T. Inoue, T. Iwai, O. Shirai and Y. Arai, J. Nucl. Mater., 299 (2001) 32-42.

[3]   K. Uozumi, M. Iizuka, T. Kato, T. Inoue, O. Shirai, T. Iwai and Y. Arai, J. Nucl. Mater., 325 (2004) 34-43.

[4]   T. Kato, M. Iizuka, T. Inoue, T. Iwai and Y. Arai, J. Nucl. Mater., 340 (2005) 259-265.

[5]   V.A. Lebedev, Selectivity of liquid metals electrodes in molten halides (in Russian), Metallurgiya, Chelyabinsk (1993).

[6]   J. Finne, G. Picard, S. Sanchez, E. Walle, O. Conocar, J. Lacquement, J.-M. Boursier and D. Noel, J. Nucl. Mater., 344 (2005) 165-168.

[7]   O. Conocar, N. Douyere, J.-P. Glatz, J. Lacquement, R. Malmbeck and J. Serp, Nucl. Sci. Eng., 153 (2006) 253-261.

[8]   O. Conocar, N. Douyere and J. Lacquement, J. Nucl. Mater., 344, 1-3 (2005) 136-141.

[9]   J. Serp, M. Allibert, A. Le Terrier, R. Malmbeck, M. Ougier, J. Rebizant and J.-P. Glatz, J. Electrochem. Soc., 152(6) (2005) 167-172.

[10]   L. Cassayre, R. Malmbeck, P. Masset, J. Rebizant, J. Serp, P. Soucek and J.-P. Glatz, J. Nucl. Mater., 360 (2007) 49-57.

[11]   P. Masset, R.J.M. Konings, R. Malmbeck, J. Serp and J.-P. Glatz, J. Nucl. Mater., 344 (2005) 173-179.

[12]   M. Iizuka, K. Kinoshita and K. Koyama, J. Phys. Chem. Solids, 66 (2005) 427-432.

[13]   S. Abousahl, P. van Belle, H. Eberle, H. Ottmar, B. Lynch, P. Vallet, K. Mayer and M. Ougier, Radiochim. Acta, 93 (2005) 147-153.

[14]   P. Masset, P.D.W. Bottomley, R.J.M. Konings, R. Malmbeck, A. Rodrigues, J. Serp and J.-P. Glatz, J. Electrochem. Soc., 152(6) (2005) 1109-1115.

[15]   K. Serrano and P. Taxil, J. Appl. Electrochem. Soc., 29 (1999) 497-503.

[16]   Y. Castrillejo, M.J. Bermejo, E. Barrado and A.M. Martinez, Electrochim. Acta, 51 (2006) 1941-1951.

[17]   Y. Castrillejo, M.J. Bermejo, A.I. Barrado, R. Pardo, E. Barrado and A.M. Martinez, Electrochim. Acta, 50 (2005) 2047-2057.

[18]   Y. Castrillejo, M.J. Bermejo, P. Diaz Arocas, A.M. Martinez and E. Barrado, J. Electroanal. Chem., 575 (2005) 61-74.

[19] A.J. Bard and L.R. Faulkner, Electrochemical methods - Fundamentals and applications, 2nd edition, John Wiley & Sons, Inc., New York (2001).

[20] Y. Castrillejo, R. Bermejo, A.M. Martinez, E. Barrado and P. Diaz Arocas, J. Nucl. Mater., 360 (2007) 32-42.

[21] P. Taxil, P. Chamelot, L. Massot and C. Hamel, J. Min. and Metal., 39, 1-2 (2003) 177-200.

[22] M.E. Kassner, M.G. Adamson, P.H. Adler and D.E. Peterson, Bulletin of Alloy Phase Diagrams, 11, 1 (1990) 82-89.

[23] P. Chiotti and J.A. Kateley, J. Nucl. Mater., 32 (1969) 135-145.

[24] V.A. Lebedev, V.I. Salnikov and I.F. Nichkov, At. Energ., 32, 2 (1972) 115-118 (in Russian).

[25] F. Lantelme, H. Alexopoulos, M. Chemla and O. Haas, Electrochim. Acta, 33, 6 (1988) 761-767.

[26] R.J.M. Konings, L.R. Morss and J. Fuger, Thermodynamic properties of Actinides, in: The Chemistry of Actinides and Transactinide Elements, 3rd Edition (J.J. Katz, L.R. Morss, J. Fuger, and N.M. Edelstein Editors), Springer, Berlin (2006) pp. 2113-2224.

[27] J.J. Roy, L.F. Grantham, D.L. Grimmett, S.P. Fusselman, C.L. Krueger, T.S. Storvick, T. Inoue, Y. Sakamura and N. Takahashi, J. Electrochem. Soc., 143(8) (1996) 2487.

[28] V.A. Lebedev, Elektrokhimiya, 14, 5 (1978) 740-742 (in Russian).

[29] L. Rault, M. Heusch, M. Allibert, F. Lemort, X. Deschanel and R. Boen, Nucl. Technol., 139 (2002) 167-174.

[30] K. Serrano, P. Taxil, O. Dugne, S. Bouvet and E. Puech, J. Nucl. Mater., 282 (2000) 137-145.

Figure Captions

Figure 1: Set-up used for electrodeposition experiments of U onto Al solid electrodes.

Figure 2: Cyclic voltammograms on W and Al (bold line) working electrodes in LiCl-KCl-UCl$_3$ ([U^{3+}] = 1.50 mass.%) at 460 °C, v=100 mV.s^{-1}.

Figure 3: Cyclic voltammograms recorded on a solid Al working electrode at 400°C in LiCl-KCl-UCl$_3$ ([U^{3+}] = 1.60 mass.%) for different scan rates.

Figure 4: Forward scans recorded on an Al electrode in LiCl-KCl-UCl$_3$ ([U^{3+}] = 1.60 mass.%) at a low scan rate (10 mV.s^{-1}) at four temperatures.

Figure 5: Open circuit chronopotentiometry curve obtained on Al solid electrode in LiCl-KCl-UCl$_3$ ([U^{3+}] = 1.46 mass.%) at 450°C. Polarization: -1.41 V/ 90 s.

Figure 6: Picture of the Al plate after chemical reductive extraction of U.

Figure 7: X-ray powder diffraction pattern of the chemical deposit of U onto Al. The symbols represent the observed points, the solid lines represent the calculated profile and the difference between observed and calculated profiles. The ticks correspond to $2\theta_{hkl}$ Bragg positions for UAl$_3$ (above) and UAl$_4$ (below).

Figure 8: Evolution of electrode potentials during galvanostatic electrodeposition of U in LiCl-KCl-UCl$_3$ ([U^{3+}] = 1.50 mass.%). Anode: U-Zr alloy, cathode: Al rod. Temperature = 460°C.

Figure 9: Al rods covered by U-Al alloy after galvanostatic electro-deposition, T=450°C, [U^{3+}] = 1.50 mass.%.

Figure 10: SEM micrograph of the cross-section of rod from run 3 (left) and EDX mapping of U, Al and Cl in the same area (right).

Figure 11: SEM micrographs of the cross-sections of Al plate cathodes alloyed with U from run U2 (left) and run U5 (right).

Figure 12: SEM-EDX determination of the molar ratio Al/U vs. the distance from the plate surface.

Tables

Table 1: Standard Gibbs energy of formation (kJ.mol^{-1}) of UAl$_n$ in the 400-550°C temperature range derived from OCP measurement after electrodeposition of U on Al in the LiCl-KCl eutectic containing UCl$_3$. Comparison to data from Kessner et al. [22].

T /°C	ΔE_{UAln} /V	$\Delta G_f°(UAl_n)$ this work	$\Delta G_f°(UAl_4)$ [22]	$\Delta G_f°(UAl_3)$ [22]	$\Delta G_f°(UAl_2)$ [22]
400	0.362 ± 0.006	-104.8 ± 1.9	-103.8	-102.6	-95.6
450	0.357 ± 0.007	-103.2 ± 2.1	-102.8	-101.4	-94.3
500	0.352 ± 0.003	-102.0 ± 0.8	-101.6	-100.4	-93.0
550	0.347 ± 0.005	-100.6 ± 1.6	-100.4	-99.2	-91.7

Table 2: Standard Gibbs energy of formation (kJ.mol^{-1}) of selected compounds and their activity coefficient in LiCl-KCl eutectic at 450°C. [*]: Activity coefficient data from Roy et al. [27] were reassessed with updated UCl_3 thermochemical data from Konings et al. [26].

Compound	$\Delta G_f°(450°C)$	$10^3 \, \gamma(450°C)$
$AlCl_3$(liq)	-547.5 [25]	0.18 [25]
UCl_3(sc, liq)	-693.5 [26]	7.3[*] [27]

Table 3: Calculation of the amount of UAl_3 and UAl_4 produced by the reaction of solid Al in equilibrium with 40g of LiCl-KCl containing 1.53 mass.%U of UCl_3.

Reaction	$\Delta_r G°(450°C)$ / $kJ.mol^{-1}$	$m(UAl_n)$ /mg
(Eq. 8) - UAl_3	44.6	19.9
(Eq. 14) - UAl_4	43.4	26.4

Table 4: Summary of the electrolysis conditions performed on solid Al rods and plates in LiCl-KCl-UCl$_3$ melt. [U^{3+}] = 1.50 mass.%.

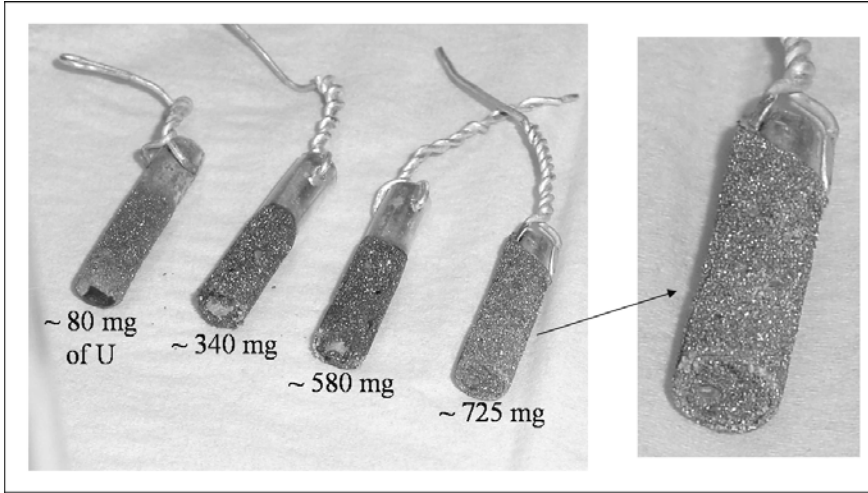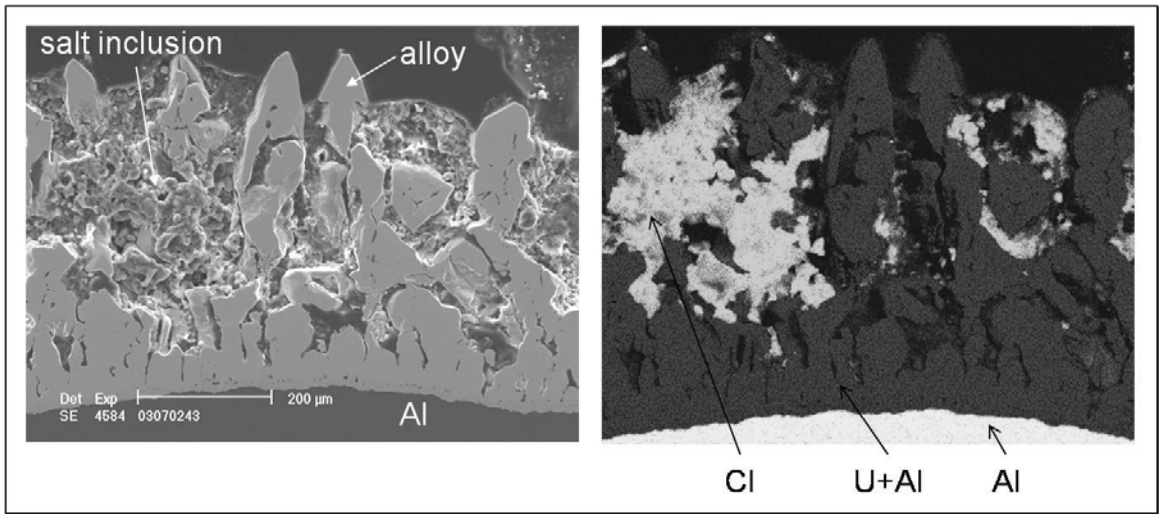| Run	T (°C)	I (A)	S (cm^2)	Q$_{total}$ (C)	m$_{th}$ (g)	Δm (g)	R (%)
Al Rods							
1	460	0.04	2.8	340	0.280	0.341	122
2	460	0.04	3.4	600	0.493	0.581	118
3	550	0.06	4	735	0.605	0.725	120
Al Plates							
U2	470	0.10	5	1100	0.905	0.904	100
U4	550	0.10	5	900	0.740	0.744	100
U5	550	0.15	5	240	0.197	0.200	102

Figures
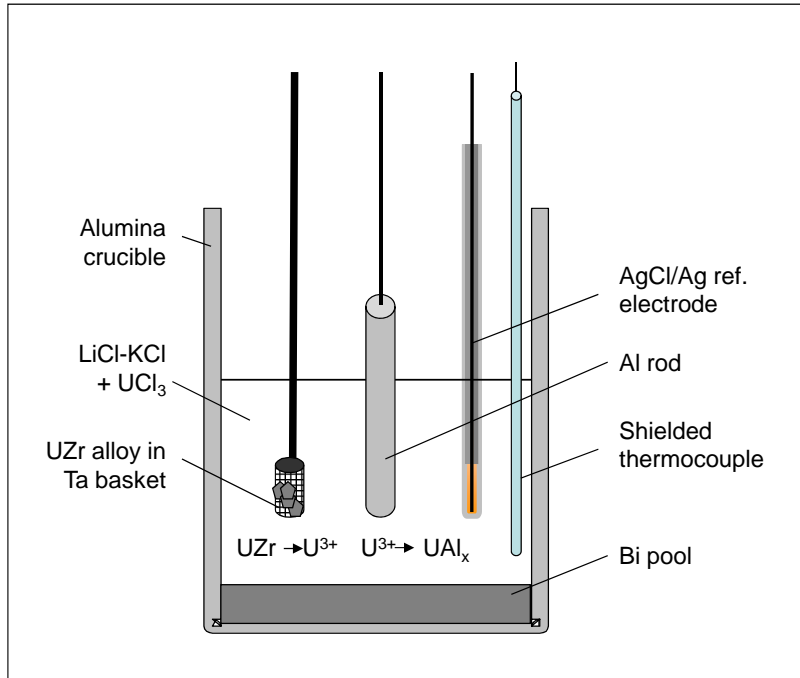
Figure 1
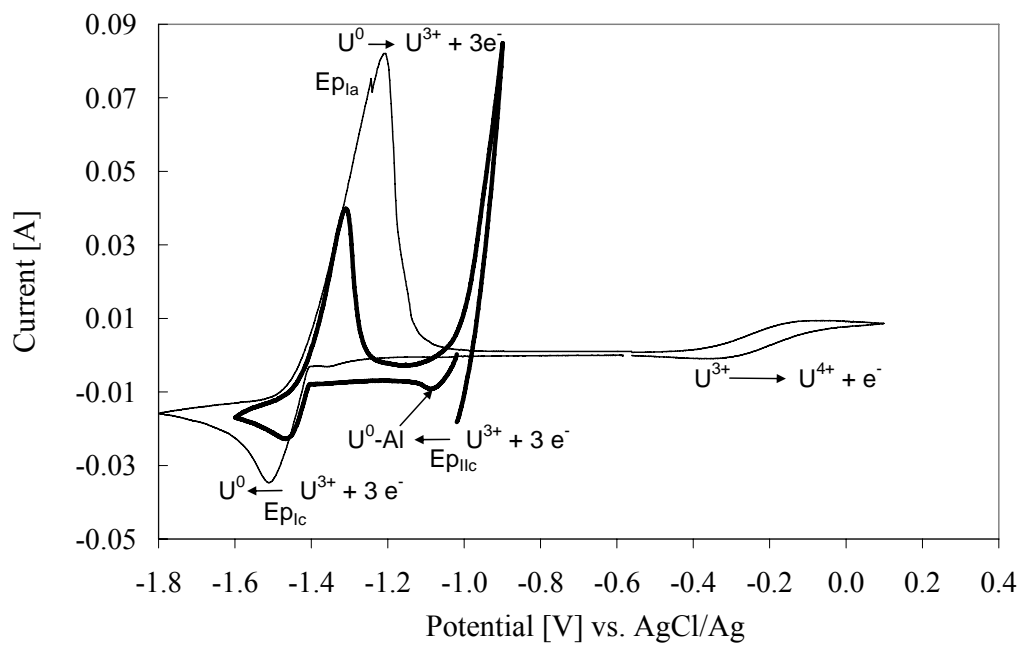
Figure 2
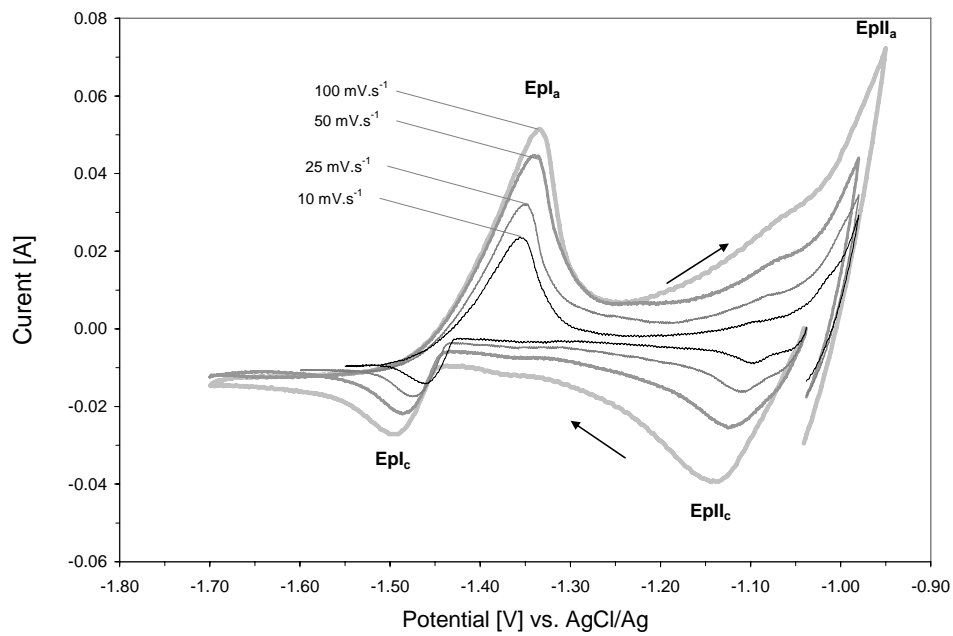
Figure 3
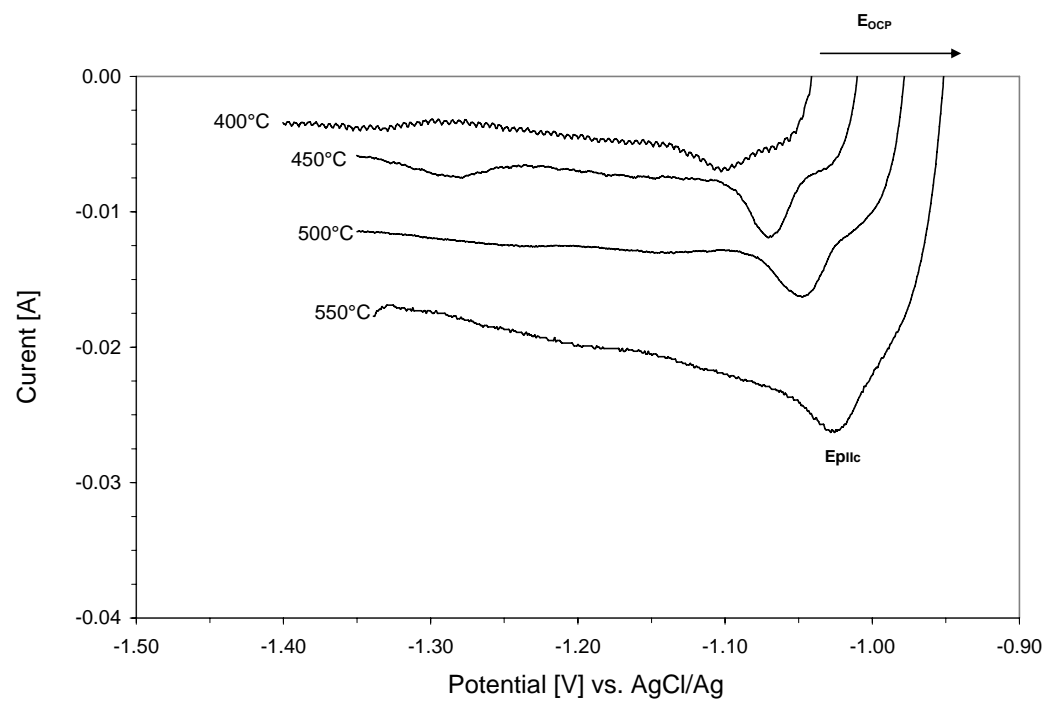
Figure 4
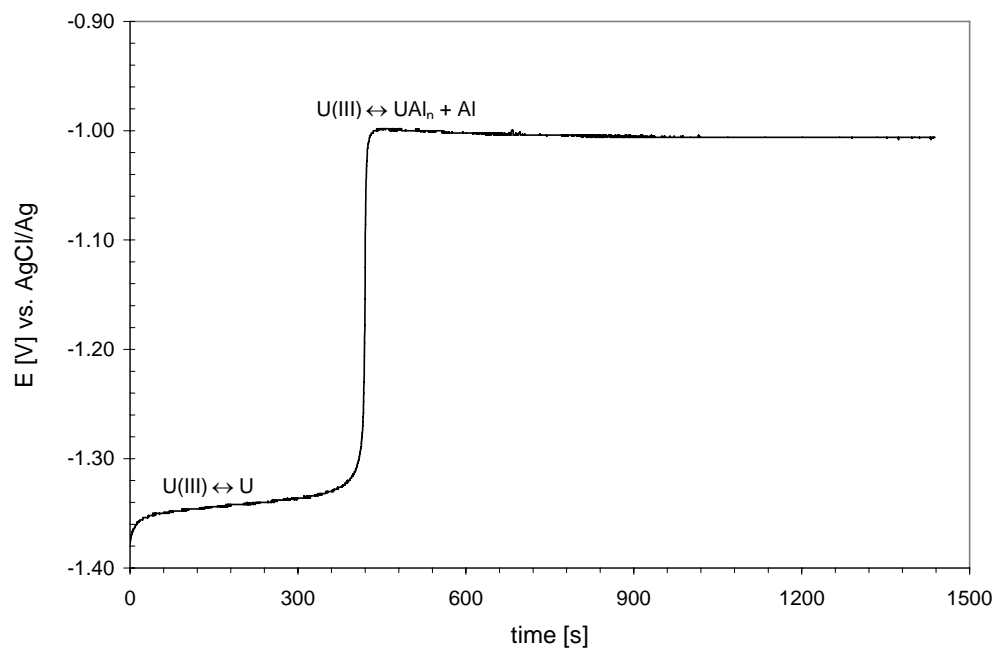
Figure 5
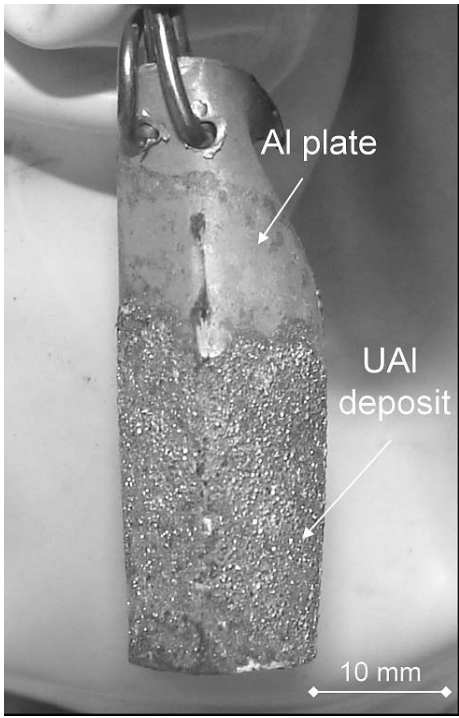
Figure 6
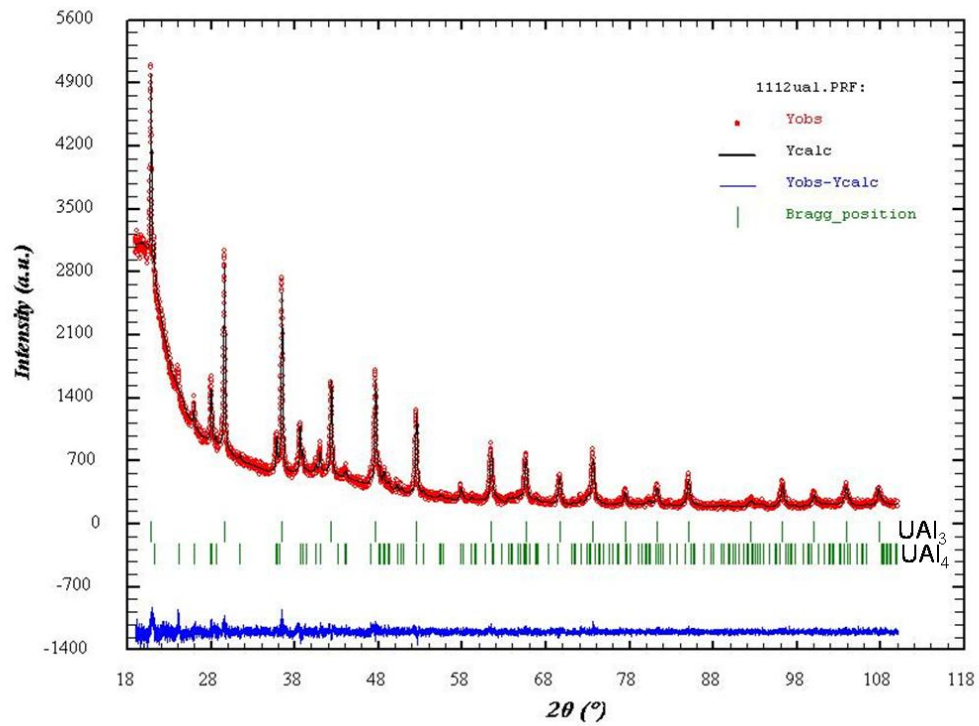
Figure 7
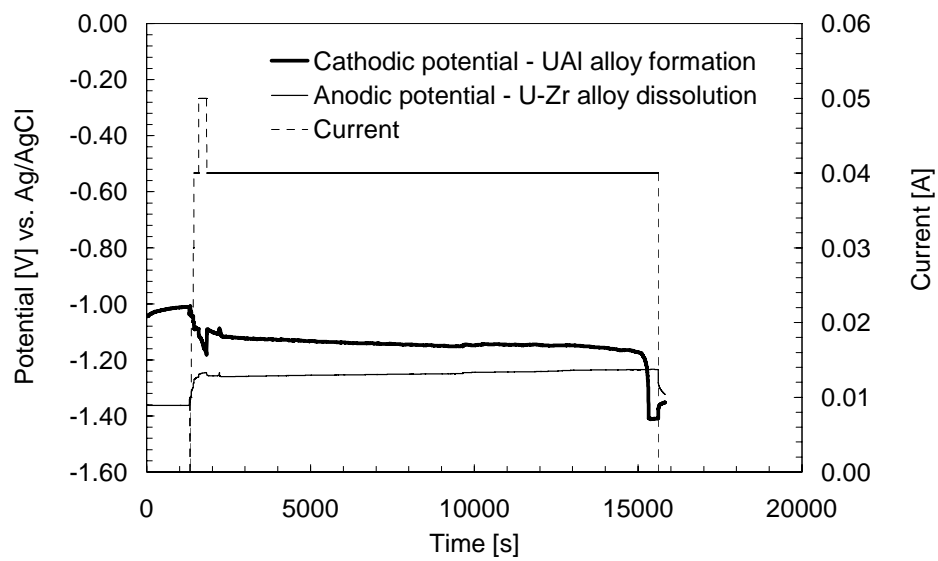
Figure 8

Figure 9

Figure 10

Figure 11

Figure 12